Residual stress near cracks of K9 glass under 1 064-nm nanosecond laser irradiation

Zhen Zhang (张 振)[1,2,3], Hongjie Liu (刘红婕)[2], Jin Huang (黄 进)[2], Xiaoyan Zhou (周晓燕)[2], Xinlu Cheng (程新路)[1], Xiaodong Jiang (蒋晓东)[2], Weidong Wu (吴卫东)[1,2,3*], and Wanguo Zheng (郑万国)[2]

[1]*Institute of Atomic and Molecular Physics, Sichuan University, Chengdu 610065, China*

[2]*Research Center of Laser Fusion, China Academy of Engineering Physics, Mianyang 621900, China*

[3]*Science and Technology on Plasma Physics Laboratory, Research Center of Laser Fusion, China Academy of Engineering Physics, Mianyan 621900, China*

[*]*Corresponding author: wuweidongding@163.com*

Received September 27, 2012; accepted November 16, 2012; posted online March 8, 2013

We present the birefringence measurements induced in K9 specimen by cracks produced by 1 064-nm Nd:YAG laser. The birefringence data are converted into units of stress, permitting the estimation of residual stress near cracks. The laser parameters and characterization of the optical material influence the value of residual stress. Residual stress in optical materials can affect fracture; thus, this factor should be considered in any formulation that involves enhanced damage resistance of optical components used in laser-induced damage experiments. The probability of the initial damage and the direction of the energy dissipation in cracks determine the residual stress distribution. Moreover, thermal-stress coupling enlarges the asymmetry of residual stress distribution. Therefore, the physical mechanism of asymmetric damage is useful for understanding the nature of optical materials under high-power laser irradiation.

OCIS codes: 140.3330, 160.6030, 140.3390, 140.3470.

doi: 10.3788/COL201311.041402.

High-power laser facilities[1], such as the National Ignition Facility in the US and the Shenguang III in China are currently being developed for inertial confinement fusion experiments and for the study of matter at extreme energy densities and pressures. In high-power laser facilities, the K9 glass is widely used as optical glass substrates. High-reflective and antireflection coatings serve as the output couplers of unstable resonators in the Nd:YAG laser systems[2]. Durable antireflective films of SiO_2 deposited on optical glass substrates with high laser-induced damage thresholds have been prepared[3]. HfO_2 thin films are typically prepared on K9 glass substrates by e-beam evaporation[4].

At 1 064-nm wavelength of the Nd:YAG pulsed laser, micrometer-scale nodule defects are the dominant causes of HfO_2 film damage. From the damage morphologies, two failure stages exist in the damage process: melting and mechanical cracking formation. In the first stage, the nanoscale impurity defect absorbs the laser energy and the temperature rapidly increases and reaches the melting point of inclusion. In the second stage, the heat-induced expansion of the impurity inclusion leads to an increase in stress. When the stresses reach the critical value, the thermal-mechanical effect breaks down the host optical material, forming circular damage craters. At low energy, the growth damage also occurs where the laser interacts with the damage area. Several reports on laser-damage effects on film threshold have been published. Negres *et al.* demonstrated that laser energy density, temporal pulse shape, and size of the site determined the rate of laser-induced damage site growth[5]. Dahmani *et al.* found that the effects of externally applied stresses enhance stress damage initiation[6]. The growth of damage sites is prevented by CO_2 laser damage mitigation[7]. After laser mitigation, residual stress near the mitigated sites can be observed. The birefringence or residual stress around the mitigation sites affects laser damage resistance.

Laser-induced cracks are useful for investigating fracture processes[8]. Tensile stresses are responsible for the mechanical failure of optical materials because most materials are weaker in tension than in compression[9]. Characterizing the residual field of stress is essential to gain accurate information; however, little effort has been exerted for the measurement of residual stress around laser-induced damage areas. One of the simplest methods to measure stress is to use a Soleil compensator[10]. This method can measure stress in a transparent specimen without any physical contact or attachment to the specimen. In this letter, residual stress was measured using the photo-elastic method. The measured residual stress is only an average value in a small area, and the maximum value is constrained by the scale range of the compensator. However, the process of measurement by this method is time-consuming and cannot measure transient stress in nanosecond resolution. Compared with other traditional methods, such as measurement with an interferometer or automated spatial scanning ellipsometer, photo-elastic method has several advantages because of its ability to measure stress without physical contact with the sample. Residual stress around the deformed area is calculated by birefringence, which is probed using a focused He–Ne laser beam. The probability of residual stress distribution was also analyzed.

Laser damage sites were created at ambient conditions using 1 064-nm Nd:YAG laser, with pulse length full-width at half-maximum (FWHM) of 6.8 ns. The beam profile was near-Gaussian, with a $1/e^2$ diameter of about

0.85 mm at the front surface of the K9 glass. The experimental setup of the laser-induced damage test is shown in Fig. 1. The output of a well-characterized stable laser was set to the desired energy and delivered to the specimen located near the focus of a focusing system. The use of a focusing system permitted the generation of destructive energy densities at the test specimen. The thickness of the K9 glass was 5 mm. The incident laser beam was sampled with a beam splitter that directed a portion of the beam to the energy calorimeter. The energy calorimeter permitted simultaneous determination of the total pulse energy. Damage sites were produced at the exit surface using single or multiple pulses. The damage morphologies from the front and lateral surfaces were imaged with two charge-coupled device (CCD) cameras after the interaction process of the nanosecond laser sample.

The birefringence induced by the residual stress field[11] emanating from the cracks was measured with a Soleil compensator (SC), as illustrated in Fig. 2. A low-power, polarized He–Ne laser beam with approximately 1-mm diameter was used as a light source, with the Soleil compensator operating in standard configuration. The linearly polarized light from the He–Ne laser was focused by a lens (L_1) on the K9 glass surface. The second lens (L_2) was used to divide the beams on the screen. The polarizer (P_1) was oriented perpendicular to the input polarization (P_2) for light extinction in the absence of the sample and the compensator. Positioned far from the cracks, the compensator was adjusted to act as a full-wave plate. Thus, combined with the polarizer, minimal light reached the screen.

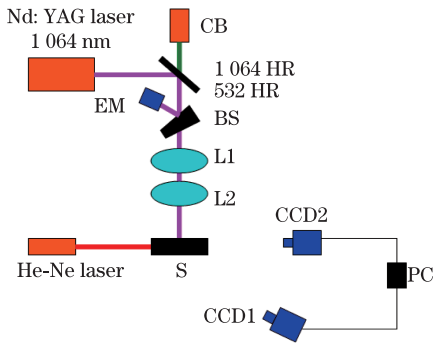

Fig. 1. Experimental setup for the laser-induced damage of K9. CB: collimated beam; HR: high reflector; AR: anti reflector; C: colorimeter; BS: beam splitter; S: K9; PC: personal computer.

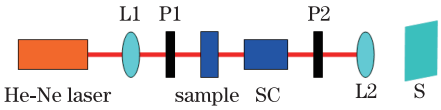

Fig. 2. Experiments setup for measuring birefringence with a SC. S: screen.

Table 1. Damage Area and Damage Depth of K9

Sample	K9 (N=15)
Energy Density (J/cm^2)	16.37
Area (μm^2)	13 800 700
Depth (μm)	2 974.68

When the He–Ne laser beam passed through the crack vicinity, adjustment of the compensator was required to maintain minimum intensity. Probing different points around the cracks at the exit surface of the K9 glass, a coarse map of birefringence signs and magnitudes were assembled.

The birefringence data can be converted to units of stress using the following equation:

$$\sigma_{\mathrm{r}}(\mathrm{MPa}) = \frac{1}{C(\mathrm{nm/cm/MPa})} \times \frac{\Gamma(\mathrm{nm})}{t(\mathrm{cm})}, \qquad (1)$$

where σ_{r} is the residual stress. The relative birefringence is defined as Γ. The stress-independent refractive index C is 35.2 nm/cm/MPa for the K9 glass in this study.

The beam was focused on the sample surface, so the irradiated area could be easily observed after each shot. The laser-induced damage threshold (LIDT) of the sample was measured in R-on-1 mode for the laser with 1 064-nm wavelength. The results indicated that the LIDT of the sample was 25.2 J/cm^2. The growth damage threshold of K9 glass was 4.3 J/cm^2. A sample with laser-induced cracks was obtained to measure the residual stress field of the K9 glass. The length and depth of the cracks were measured by optical microscopy, as shown in Table 1. Growth damage occurred when the laser energy density fell far below the damage threshold while the pulse number was gradually increased.

The damage morphology of K9 is depicted in Fig. 3, where the energy density is 16.37 J/cm^2 and the pulse counts are 15. The damage radius of the K9 glass under high laser energy density is about 2.1 mm. The damage crater consists of a core of molten nodules with a botryoidal morphology and fibers evident of a thermal explosion, followed by quenching from liquid state at this high-energy absorption region. The molten core is concentrically surrounded by an annulus of fractured material, indicative of mechanical damage accompanied by spallation of material.

The positive direction along the x and y axes was defined, as shown in Figs. 3(a) and (b). The compensator was adjusted far from the crack to act as a full-wave plate. Thus, combined with the polarizer, minimal light reached the screen. Moving off an undamaged sample site and repeatedly returning to it, the repeatability of the system was about 0.57 nm. The maps of the birefringence along the x axis were built by aligning the He–Ne laser beam onto different points on the K9 surface. The laser parameters and characterization of material influence the shockwave distribution of optical components. The residual stress in the birefringence unit in the K9 glass along the x axis was measured.

The energy density of the laser pulse was near the damage threshold of the optical material when used in high-power laser systems. When the laser energy density is below growth damage threshold and above damage threshold, the investigation of the residual stress distribution has little engineering values. The birefringence around laser-induced cracks with pulse number (N = 15) at an energy density of 16.37 J/cm^2 was measured. When y is a constant value, the birefringence distribution in K9 glass is as described in Figs. 4 and 5. A residual tensile-stress field around the crack exists when the value of y is zero. Compressive stress was also observed (y =

+5). The changing direction of the residual stress from tensile stress to compressive stress reveals the characteristics of shockwave transmission in optical material.

Figure 5 shows that the birefringence is very close to the crack and continuously decreases over a finite distance until the crack effect vanishes. The finite distance is about 2 mm for K9 glass under high-energy density laser irradiation. The maximum value of birefringence is about 160 nm, whereas the minimum value is about 0. The existence of a residual compressive stress field around a crack produced by laser irradiation is clearly depicted in Fig. 5. The maximum compressive stresses are located in the first and third quadrants. With an increase in the value of y, the minimum value of birefringence rapidly increases from –20 to 160 nm. The anti-symmetry of the birefringence was also observed. The cracks are located in the same quadrant (Fig. 3), which is consistent with the results of Fig. 5.

When laser counts are constant, laser energy density is an important factor that can influence the distribution of residual stress. After laser-induced damage, compressive stress and tensile stress are observed. The sample exhibits the highest birefringence closest to the cracks. The birefringence decreases over a finite distance until the crack effect vanishes. The laser-induced damage growth of the K9 glass is influenced by compressive stress and tensile stress after the shockwave is transmitted in optical components. Compressive stresses are responsible for the mechanical failure of specimens. When the energy density of an input laser pulse is above a certain threshold value and under subsequent cyclic laser shots, microscopic volume changes give rise to mechanical compressive stresses. Different shapes of residual stress along the y axis in different damage areas may be explained by the different damage mechanisms in K9 glass.

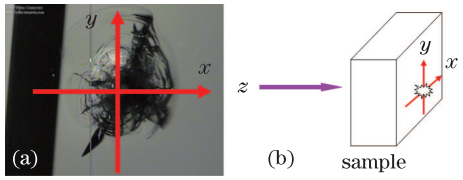

Fig. 3. (a) Laser-induced damage morphology of K9 glass recorded by CCD camera; (b) definition of the direction.

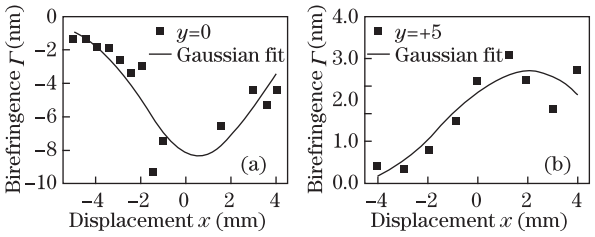

Fig. 4. Birefringence on the surface of K9 glass when the value of y is 0 or 5 mm.

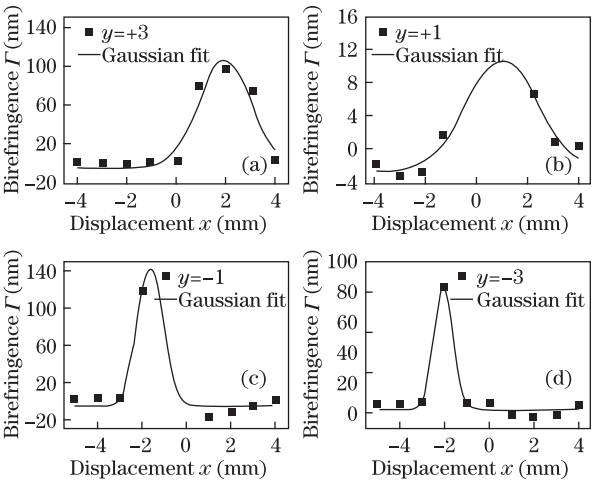

Fig. 5. Birefringence on the surface of K9 glass when the absolute value of y is 1 or 3 mm

When high-energy density laser irradiates the K9 glass, it undergoes explosion of metal inclusion and the subsequent ejection of bulk K9 glass. As a result, surface morphology modifications such as voids and cracks form, as depicted in Fig. 3. Shockwaves generated by phase explosion further compress the bulk material. The competition between the rate of energy redistribution and energy diffusion[12] to the surrounding atoms determines the energy deposition process. Resonance absorption and collisions dominate the absorption process[13]. At the local heating stage, the displacement of atoms in the lattice and their velocities are small. When the sample is rapidly cooled, thermal shock results in the development of compressive stress in the laser-irradiated area[14]. Furthermore, shockwaves generated by phase explosion will further compress the bulk material. Due to the restraint of the surrounding material, compressive stress is developed. After laser irradiation, higher compressive stress may be released. The presence of compressive stress is clearly depicted in Figs. 4 and 5. These mechanical stresses induce birefringence in K9 glass. The residual stress results reflect the occurrence in bulk K9 glass after laser irradiation. Compressive stress governs crack development and fatigue properties[15].

The statistical nature of the failures of optical components subjected to laser irradiation is a major challenge in high-power laser systems. The unpredictable fatigue lives of the optical materials arise from the Poisson distribution of low populations of microscale defects[16]. Based on a novel rheological model of fracture, the behavior associated with fracture is a consequence of the coupling between shear-induced density fluctuations and deformation fields[17]. An analytical model[18] was developed to explain the crack arrest in fused silica obtained by the breakage of this hoop-stress symmetry. Thus, the probability of the initial damage and the direction of energy dissipation in cracks determine the residual stress distribution. Thermal-stress coupling enlarges the asymmetry of residual stress distribution. The Hoop model is not suitable for the exploration of residual stress distribution of optical material under nanosecond laser irradiation. The experimental results revealed that the Hoop model should be revised. Some efforts can be exerted, such as a special fracture structure interacting with the input laser. The effect of light and thermal-mechanical interaction should be considered in investigating the nature of residual stress evolution.

In conclusion, residual stress near the cracks of the K9 glass under 1 064-nm nanosecond laser irradiation is measured by photo-elastic method. The difference

of residual stress near cracks of the optical material is also discussed. The probability of initial damage and the direction of energy dissipation in cracks determine the residual stress distribution. Thermal-stress coupling enlarges the asymmetry of residual stress distribution. Therefore, the physical mechanism of asymmetric damage is useful in studying the nature of optical materials under high power laser irradiation.

This work was supported by the National Natural Science Foundation of China (No. 61078075) and the Development Foundation of Science and Technology for China Academy of Engineering Physics (Nos. 2010B0401055 and 2011B0401065). The authors wish to thank Dahua Ren and Xinyou An for their experimental assistance in the Research Center of Laser Fusion in China.

References

1. K. B. Aime, C. Belin, L. Gallais, P. Grua, E. Fargin, J. Neauport, and I. Toven-Pecault, Opt. Express **17,** 18703 (2009).
2. C. Giuri, M. R. Perrone, and V. Piccinno, Appl. Opt. **36,** 1143 (1997).
3. Y. Xu, L. Zhang, D. Wu, Y. Sun, Z. Huang, X. Jiang, X. Wei, Z. Li, B. Dong, and Z. Wu, J. Opt. Soc. Am. B **22,** 905 (2005).
4. D. Zhang, C. Wang, P. Fan, X. Cai, Z. Zheng, J. Shao, and Z. Fan, Opt. Express **17,** 8246 (2009).
5. R. A. Negres, Z. M. Liao, G. M. Abdulla, D. A. Cross, M. A. Norton, and C. W. Carr, Appl. Opt. **50,** D12 (2011).
6. F. Dahmani, J. C. Lambropoulos, A. W. Schmid, S. Papernov, and S. J. Burns, Appl. Opt. **38,** 6892 (1999).
7. L. Gallais, P. Cormont, and J. L. Rullier, Opt. Express **17,** 23488 (2009).
8. Y. Z. Li, M. P. Harmer, and Y. T. Chou, J. Mater. Res. **9,** 1780 (1994).
9. D. Albagli, M. Dark, L. T. Perelman, C. von Rosenberg, I. Irzkan, and M. S. Feld, Opt. Lett. **19,** 1684 (1994).
10. J. E. Logan, N. A. Robertson, and J. Hough, Opt. Commun. **107,** 342 (1994).
11. F. Dahmani, A. W. Schmid, J. C. Lambropoulos, and S. Burns, Appl. Opt. **37,** 7772 (1998).
12. I. Santos, L. A. Marques, and L. Pelaz, Phys. Rev. B **74,** 174115 (2006).
13. C. T. Hansen, S. C. Wilks, and P. E. Young, Phys. Rev. Lett. **83,** 5019 (1999).
14. C. Barnes, P. Shrotriya, and P. Molian, Int. J. Mach. Tool. Manufact. **47,** 1864 (2007).
15. X. Zhang, E. J. Ashida, S. Shono, and F. Matsuda, J. Mater. Process. Technol. **174,** 34 (2006).
16. K. S. R. Chandran, Nature Mater. **4,** 303 (2005).
17. A. Furukawa and H. Tanaka, Nat. Mater. **8,** 601 (2009).
18. F. Dahmani, J. C. Lambropoulos, A. W. Schmid, S. Papernov, and S. J Burn, Appl. Opt. **38,** 6892 (1999).